Numerical and experimental study of horizontal pneumatic transportation of spherical and low-aspect-ratio cylindrical particles

Numerical and Experimental Study of Horizontal Pneumatic Transportation of Spherical and Low-Aspect-Ratio Cylindrical Particles

Mohammadreza Ebrahimi, Martin Crapper and Jin.Y.Ooi

School of Engineering, The University of Edinburgh, King's Buildings, Edinburgh, EH9 3JL, UK

Emails: M.Ebrahimi@tugraz.at
Martin.Crapper@ed.ac.uk
J.Ooi@ed.ac.uk

1. **Introduction**

This study was conducted as a part of the PARDEM project, an EU-funded, Framework 7 Marie Curie Initial Training Network, with the intention of validating the CFD-DEM method to establish its predictive capability.

A wide range of industrial processes involve multiphase granular flows. These include catalytic reactions in fluidized beds, the pneumatic conveying of raw materials and gas-particle separators. Due to the complex nature of multiphase flows and the lack of fundamental understanding of the phenomena in a multiphase system, appropriate design and optimized operation of such systems has remained a challenging field of research. Design of these processes is hampered by difficulties in upscaling pilot scale results, the difficulties involved in experimental measurements and in finding reliable numerical modelling methods.

Various non-intrusive measurement techniques have been introduced and applied for gas-particle flows such as particle tracking velocimetry [1], particle image velocimetry (PIV) [2], photographic image techniques [3], CCD cameras [4], phase Doppler anemometry (PDA) [5], electrical capacitance tomography (ECT) [6, 7], laser Doppler anemometry (LDA) [8, 9], and radioactive particle tracking [10]. Detailed information from these measurement techniques provides useful insight into system design and optimization. In this study the LDA

technique has been applied. The LDA technique is one of the most commonly used experimental tools for use in gas and particle situations, as it is non-intrusive, optical and can handle velocity components with high temporal and spatial resolution, even in highly turbulent flows. LDA measurements have previously been applied to investigate gas-solid flows in pneumatic conveying systems [11-14]. Table 1 lists the studies in which the LDA technique has been applied to investigate horizontal pneumatic conveying systems. Brief key results of each study also are presented in this table.

Generally, multiphase systems such as pneumatic conveying systems can be described by two different numerical models, namely Eulerian-Eulerian (E-E) or Eulerian-Lagrangian (E-L) approaches. The particle concentration, the nature of the system and the level of information required from the results decide the appropriate method for simulation.

In this study the Eulerian-Lagrangian method known as coupled Computational Fluid Dynamics and Discrete Element Method (CFD-DEM) is used. Particles are described as discrete entities and Newton's equations of motion are solved to track each individual particle. The averaged Navier-Stokes equations are solved to describe the continuous phase. The conservation equations (continuity and momentum) are integrated over the Eulerian grid that covers the entire domain. Momentum exchange between the particle and fluid phases facilitates the coupling.

In one of the first attempts to apply DEM for numerical modelling of pneumatic conveying, Tsuji et al. [16] applied 1D CFD and 3D DEM to model a horizontal pipe. The Ergun equation was used to calculate the fluid force acting on the particles. Due to the CPU time limitations, they used large particles (d_p=10 mm) and a small number of particles in a short pipe. Lun and

Liu [17] performed CFD-DEM modelling for a dilute horizontal particle-laden channel flow for a low particle volume fraction in order of 10^{-3}. They concluded that the particle-particle collisions and Magnus lift force had crucial effects to keep particles suspended in the channel. They ignored the influence of the dispersed phase on the carrier phase turbulence and a conventional k-ε was applied in the simulation. Fraige and Langston [18] developed Tsuji's model [16] by correcting the pressure drop calculation in pneumatic conveying for 1D CFD and 3D DEM simulation. It was assumed that the fluid flow was at steady state for each time step. The model could then successfully reproduce various flow patterns. Kuang and Yu [19] could predict the various flow regimes in 3D horizontal pneumatic conveying. However, they did not consider gas phase turbulence alteration due to the presence of the dispersed phase.

Lun [20] compared simulation results of mean gas and particle velocities and carrier phase turbulence intensity with the experimental measurements of Tsuji et al. [21] for a dilute steady state flow in vertical pneumatic conveying. A modified k-ω turbulence model was used to take into account the effect of particles on the fluid phase turbulence level. A drag model suggested by Clift and Gauvin [22] was applied. The model could predict reasonably the mean gas and particle velocities. However, it only could capture the gas turbulence level trend qualitatively in the pipe. Laín et al. [11] applied Reynolds-averaged conservation equations in connection with a full Reynolds stress turbulence model to describe the fluid phase. Particle-particle collisions were modelled using a stochastic approach [23] and the wall roughness was also taken into account to simulate the particle-wall collisions [1]. Good agreement between experimental results by PDA and simulation results for the mean and root mean square (RMS) velocities of gas and particles in a 2D horizontal channel was observed. Laín and Sommerfeld [12] applied the model developed by Laín et al. [11] to investigate the pressure drop and gas and particle interaction in a 2D dilute horizontal channel. Turbulence

reduction by 130 and 195 μm particles was captured by model with reasonable consistency with the experiments. They also concluded that the pressure drop increased by increasing the particle mass loading, particle size and wall roughness, due to the increased particle-wall collision frequency.

Particle shape is known to play a significant role on the particle-fluid interaction and particle dispersion in a two-phase flow and has been the subject of investigation in literature [24-27]. Rosendahl [25] showed that the trajectories of cylindrical and ellipsoidal particles are different from spheres in a horizontal combustor. Hilton and Cleary [26] and [28] investigated the effect of particle shape on flow regime in pneumatic conveying. They concluded that the particle shape had a significant influence on the bulk flow. Laín and Sommerfeld [27] performed a study on the dilute pneumatic conveying of non-spherical particles in a horizontal channel using PDA to measure gas and particle velocities. In their numerical model, the particles were assumed to be isometric (low-aspect-ratio) with the ratio of the maximum length to the minimum length below 1.7. Particle rotation and particle-particle interaction were neglected and lift force was not modelled. A qualitatively good comparison between experimental data and numerical simulation was observed. Readers are referred to reference [29] for more information regarding the motion of non-spherical particles in a shear flow, during sedimentation and turbulent flow. A comprehensive review of the modelling of motion of non-spherical particles in a two-phase flow also was summarized by Mandø et al. [30].

The aim our research was to perform detailed experiments using laser Doppler anemometry (LDA) and corresponding numerical simulations using a coupled CFD-DEM approach and thus to quantify the predictive capability of CFD-DEM for particles of differing shape in a

horizontal pneumatic conveying system. A secondary aims was to provide a detailed experimental data set covering a wide range of flow conditions in pneumatic conveying to supplement the limited number currently available in the literature.

2. **Experimental Procedure and Measurements**

Figure. 1 displays a schematic sketch of the horizontal pneumatic conveying apparatus consisting of an inlet arrangement where the particles are fed from a hopper with a screw feeder, the conveying line and an exit with a cyclone for separating out the particles and a fan. The particles enter the horizontal conveying line via a pipe inclined at 45°. The length of the inclined pipe is 0.35 m. Once inside the horizontal pipe, the fan sucks both the air and the particles into the cyclone, where the gas and particles are separated. The horizontal conveying section is 6.5 m long and is connected to the vertical section (1.2 m) with a bend. The pipe internal diameter is 0.075 m. Both gas and particle measurements were carried out at two different cross sections in the horizontal section (as shown by the red arrows) at distances of z=1 m and z=2 m from the point where the particles are introduced into the horizontal section (z being the longitudinal coordinate). The particle flow rate can be regulated by adjusting the screw feeder revolutions per minute (RPM) and the air flow rate can also be regulated, making it possible to obtain the desired solid loading ratio (SLR = solid mass flow rate/gas mass flow rate) in the conveying line.

The LDA system used in the experiments can measure only one velocity component at a time. The wavelength of the laser light is equal to 514 nm. The backscatter mode was used for all the experiments. The transmitting and receiving lens focal lengths are 800 mm. The laser beams are refracted while passing through the pipe curved wall. As a result, there would be a deviation between the actual beams intersection point and the expected position which needs

to be considered [13] and [31]. The LDA system is mounted on a 3D traverse system allowing measurement at different locations. It should be noted that the LDA can only collect data at one point at a time. However, by moving the measurement point along a cross section, a profile measurement for the cross section is achieved. The first velocity measurement was at the pipe centre, and then the probes were moved horizontally or vertically to measure the gas and particle velocities for other measurement points across the pipe.

The measurement reproducibility was checked by repeating the measurements three times, and each measurement was carried out for 50 seconds. The maximum number of samples for each measurement point was set to 5,000 for particle laden flows. To measure the gas velocity, the carrier phase was impregnated by seeding particles in the form of incense smoke. Smoke was added to the air at the beginning of the horizontal line. The particle velocity measurement was performed separately by adding particles. Simultaneous measurement of gas and particle velocities was carried out. For this, incense smoke and particles were injected into the pipe simultaneously. The large size of solid particles compared to the smoke particles ensured clearly distinguishable measurement of both gas and particle velocity.

Glass beads in three different sizes (0.8-1 mm, 1.5 mm and 2 mm) with a particle density of 2540 kg/m^3, and cylindrical polyamide with a nominal size of 1×1.5 mm and a particle density of 1140 kg/m^3 were chosen for the research. These particle sizes give a reasonable time step in the numerical work and guarantee a reasonable computational time. For the spherical glass beads, the particle flow rates were set to 0.1128 kg/s, 0.1277 kg/s and 0.1329 kg/s. For the cylindrical Polyamide, the particle flow rates were fixed at 0.0296 kg/s and 0.04467 kg/s. For spherical glass beads, the resulting SLRs in the experiments were 2.3, 3.0 and 3.5. For

cylindrical polyamide, SLRs were 0.6, 1.0 and 1.2.The detailed experimental data arising from our study has been archived and is available for future researchers [32].

3. **Numerical Approach and Models**

Coupled CFD-DEM In this study are carried out using the commercial software Ansys FLUENT version 12.1 and EDEM version 2.4 in an Eulerian-Lagrangian framework in which particles are tracked individually. Additional functionality was introduced to the commercial software where needed by means of Applications Programmer Interface (API) coding. The locally averaged Navier-Stokes equations are solved in FLUENT for the carrier phase using a finite volume discretisation scheme and applying an iterative solution procedure based on the SIMPLE algorithm. The motion of the particle phase in the simulation is described by solving Newton's laws of motion in EDEM. The two software codes are then coupled with full momentum exchange between the solid and fluid phases (Two-way coupling) as described below.

3.1. Mathematical Formulation of the Fluid Phase

The locally averaged Navier-Stokes equations derived by Anderson and Jackson [33] are solved to model the fluid flow. The time dependent three dimensional mass and momentum conservation equations may be written as follows:

$$\frac{\partial}{\partial t}(\varepsilon_f \rho) + \nabla.\left(\varepsilon_f \rho \bar{v}\right) = 0 \tag{1}$$

$$\frac{\partial}{\partial t}\left(\varepsilon_f \rho \bar{v}\right) + \nabla.\left(\varepsilon_f \rho \bar{v} \bar{v}\right) = -\nabla \mathrm{p} + \nabla.\left(\varepsilon_f \tau\right) + \nabla.\left(\varepsilon_f \tau'\right) + \varepsilon_f \rho g - S \tag{2}$$

$$S = \frac{\sum_i^{n_m} F_{interaction,i}}{\Delta V_{mesh}} \tag{3}$$

where ρ is the fluid density and ε_f is the porosity in an Eulerian grid; τ is the fluid viscous stress tensor and τ' is the Reynolds stress tensor; n_m and ΔV_{mesh} are the number of particles in a computational cell and the computational cell volume respectively; S is the volumetric force acting on each mesh cell and $F_{interaction}$ includes drag and lift forces in this study.

3.1.1 **Drag Modelling**

The Ergun [34] and Wen and Yu [35] drag models were used for modelling the aerodynamic force acting on spherical particles:

$$\beta = 150\frac{(1-\varepsilon_f)^2}{\varepsilon_f}\frac{\mu}{d_p^2} + 1\ .75(1-\ \varepsilon_f)\frac{\rho}{d_p}\left|(v-u_p)\right| \quad \varepsilon_f < 0.8 \tag{4}$$

$$\beta = \frac{3}{4}\frac{C_D}{d_p}\rho(1-\varepsilon_f)\varepsilon_f{}^{-2.7}\left|v-u_p\right| \quad \varepsilon_f > 0.8 \tag{5}$$

$$F_D = \frac{V_p\beta}{1-\varepsilon_f}(v-u_p) \tag{6}$$

where μ is the fluid viscosity. C_D is calculated as follows:

$$C_D = \begin{cases} 24/Re_p & Re_p \le 0.5 \\ \dfrac{24\left(1+0.15Re_p^{0.687}\right)}{Re_p} & 0.5 < Re_p \le\ 1000 \\ 0.44 & Re_p > 1000 \end{cases} \tag{7}$$

For simulating the non-spherical particles, the drag model proposed by Di Felice [36] was applied as previously implemented by Hilton and Cleary [37].

$$\xi = 3.7 - 0.65exp\left(-\frac{\left(1.5 - log_{10}Re_p\right)^2}{2}\right) \tag{8}$$

$$f(\varepsilon_f) = \varepsilon_f{}^{-\xi} \tag{9}$$

$$F_D = \frac{1}{2} C_D A\rho \left|(v - u_p)\right| (v - u_p) f(\varepsilon_f) \tag{10}$$

The influence of shape on drag coefficient (C_D) was considered by the sphericity (ψ) shape factor. The drag coefficient suggested by Haider and Levenspiel [38] and Ganser [39] was applied as given in equations (11) and (13) respectively, this being regarded as sufficient given that the sphericity of the Polyamide particles was (ψ =0.8585).

More sophisticated drag coefficients which are function of particle orientation can also be used. However, since the sphericity of the non-spherical particles studied in this study is close to unity (ψ =0.8585), the above mentioned drag coefficients are appropriate to be implemented. For the same reason, the influence of non-spherical particle orientation on the aerodynamic forces and torques was neglected.

$$C_D = \frac{24}{Re_p}\left(1 + ARe_p^B\right) + \frac{C}{1 + \frac{D}{Re_p}} \tag{11}$$

Where

$$A = \exp(2.3288 - 6.4581\psi + 2.4486\psi^2)$$

$$B = 0.0964 + 0.5565\psi \tag{12}$$

$$C = \exp(4.905 - 13.8944\psi + 18.4222\psi^2 - 10.2599\psi^3)$$

$$D = \exp(1.4681 + 12.2584\psi - 20.7322\psi^2 + 15.8855\psi^3)$$

where Re_p is calculated based on the equal volume sphere diameter, i.e. $d_e = \sqrt[3]{6V_p/\pi}$

$$C_D = \frac{24}{Re_p K_1}\left\{1 + 0.1118\left(Re_p K_1 K_2\right)^{0.6567}\right\} + \frac{0.4305}{1 + {}^{3305}/_{Re_p K_1 K_2}} \tag{13}$$

Here Re_p is calculated based on the equal volume sphere diameter, and K_1 and K_2 are functions of sphericity, and are calculated as:

$$K_1 = \left[\left(d_n/3d_p\right) + (2/3)\psi^{-0.5}\right]^{-1}$$

$$K_2 = 10^{1.8148(-log\psi)^{0.5743}} \tag{14}$$

where d_n is the equal projected area circle diameter. Following Ganser [39], d_n in equation (14) is replaced by 1 for the isometric (low-aspect-ratio) shape. The projected area in the drag force calculation was determined based on the equal volume sphere diameter (d_e) whilst the voidage function in the Di Felice drag model [36] (which takes account of the presence of surrounding particles) was using the equal volume sphere diameter [28].

3.1.2 **Lift Modelling**

In our previous study [40], it was found that for spherical particles, the inclusion of Magnus lift force due to particle rotation was essential to reproduce the general behaviour observed in the experiments. In view of this we implemented Magnus lift force in all the simulations in this research,, taking the view that since the non-spherical particles were of low aspect-ratio (ψ =0.8585) it was reasonable to apply the same formulation as for the spherical particles. The equations used to represent Magnus lift were [41]:

$$F_{Magnus} = 0.125\pi d_p^3 \rho \frac{Re_p}{Re_\Omega} C_L\left[\left(\omega_p - 0.5\omega_c\right) \times \left(v - u_p\right)\right] \tag{15}$$

$$C_L = 0.45 + \left(\frac{Re_p}{Re_\Omega} + 0.45\right)\exp(-0.0568 Re_\Omega^{0.4} Re_{\mathrm{p}}^{0.3}) \tag{16}$$

where C_L and ω_c are coefficient of Magnus lift force and fluid vorticity, respectively. Re_Ω is a particle rotation Reynolds number given by

$$Re_\Omega = \frac{\rho\left|\omega_p - 0.5\omega_c\right| d_p^2}{\mu} \tag{17}$$

3.1.3 **Turbulence Modelling**

We selected the k-ε turbulence model as a basis for our simulations for three reasons. Firstly, in using commercial software the choice of model was limited when coupling the CFD and DEM products; secondly test runs with more complex turbulence models, in particular the Reynolds Stress Model, proved too expensive on computer time to have any practical use, and thirdly literature exists on which to base the calculation of modulation of fluid phase turbulence when using the k-ε model, whereas there is no previous work on implementing this for other turbulence models.

The general k-ε turbulence model equations in FLUENT are as follow [42]:

$$\frac{\partial}{\partial t}(\rho k) + \frac{\partial}{\partial x_i}(\rho k v_i) = \frac{\partial}{\partial x_i}\left[\left(\mu + \frac{\mu_t}{\sigma_k}\right)\frac{\partial k}{\partial x_i}\right] + G_k + G_b - \rho\varepsilon - Y_M + S_{kp} \tag{18}$$

$$\frac{\partial}{\partial t}(\rho \varepsilon) + \frac{\partial}{\partial x_i}(\rho \varepsilon v_i) = \frac{\partial}{\partial x_i}\left[\left(\mu + \frac{\mu_t}{\sigma_\varepsilon}\right)\frac{\partial \varepsilon}{\partial x_i}\right] + C_{\varepsilon 1}\frac{\varepsilon}{k}(G_k + C_{\varepsilon 3}G_b) - C_{\varepsilon 2}\rho\frac{\varepsilon^2}{k} + S_{\varepsilon p} \tag{19}$$

where $\mu_t = \rho C_\mu k^2/\varepsilon$ is the turbulent viscosity, σ_k and σ_ε are turbulent Prandtl numbers and S_{kp} and $S_{\varepsilon p}$ are user defined source terms. The model constants have values as set out in Table 2.

In this study the source terms proposed by Geiss et al. [43] and Mandø [44] for spherical particles are implemented in the CFD-DEM code by the User Defined Functions (UDFs), in order to take into account the influence of the dispersed phase on the carrier phase. These source terms can be written as follows:

$$S_{kp} = \frac{\phi_p \rho_p}{\tau_p}\left(\left|\overline{v_i} - \overline{u_{pi}}\right|^2 - 2k\right) \tag{20}$$

$$S_{\varepsilon p} = C_{\varepsilon 3}\frac{\varepsilon}{k} S_{kp} \tag{21}$$

The empirical constant $C_{\varepsilon 3}$ does not have a unique value and various values have been proposed ranging from 1.0 to 2.0 [45].

It should be noted that for all our simulations, the Stokes number is >>1. Therefore, the change in the turbulence structure does not have a significant influence on the particle flow pattern, so the turbulence modulation is a one-way process.

The literature contains no information about the carrier phase turbulence modulation due to non-spherical particles [27]. Therefore, the conventional k-ε turbulence model was applied in the simulations without alteration.

4. **Mathematical Formulation of the DEM**

Translational and rotational motions of particles in EDEM software are described by the equations below.

$$m_i \frac{du_{p,i}}{dt} = m_i g + \sum_{j=1}^{k_i} F_{c,ij} + F_{interaction,i} \tag{22}$$

$$I_i \frac{d\omega_{p,i}}{dt} = \sum_{j=1}^{k_i} T_{ij} \tag{23}$$

where $F_{c,ij}$ is the contact force and $F_{interaction,i}$ includes drag and lift forces; $u_{p,i}$ and $\omega_{p,i}$ are the linear and angular particle velocities; m_i, I_i, and T_i denote the mass and the moment of inertia of the particle and the torque acting on a particle respectively. For more information regarding

how the particle mass and particle moment of inertia are calculated please refer to the EDEM tutorial [46].

The EDEM code deploys the soft contact approach whereby a non-linear Hertz-Mindlin contact model is used to model the particle-particle and particle-geometry contacts. The normal component of a contact force can be expressed as follows, and are functions of normal overlap δ_n, equivalent Young's modulus Y^* and equivalent radius R^*.

$$F_n = \frac{4}{3} Y^* \delta_n^{3/2} \sqrt{R^*} \tag{24}$$

$$\frac{1}{Y^*} = \frac{(1-\nu_i^2)}{Y_i} + \frac{(1-\nu_j^2)}{Y_j} \tag{25}$$

$$\frac{1}{R^*} = \frac{1}{R_i} + \frac{1}{R_j} \tag{26}$$

Y, ν and R are Young's modulus, Poisson's ratio and particle radius respectively; subscripts i and j represent the particles in contact. The normal damping force is given by

$$F_n^d = -2\sqrt{5/6}\,\gamma \sqrt{S_n m^*} V_n^{rel} \tag{27}$$

$$S_n = 2Y^* \sqrt{R^* \delta_n} \tag{28}$$

and

$$\gamma = \frac{\ln e}{\sqrt{\ln^2 e + \pi^2}} \tag{29}$$

$$\frac{1}{m^*} = \frac{1}{m_i} + \frac{1}{m_j} \tag{30}$$

where m^* is the equivalent mass, e is the coefficient of restitution, S_n is the normal stiffness, and V_n^{rel} is the normal component of the relative velocity between the particles.

Tangential force and damping are calculated by the following equations [47]:

$$F_t = -S_t \delta_t \tag{31}$$

$$S_t = 8G^* \sqrt{R^* \delta_n} \tag{32}$$

$$F_t^d = -2\sqrt{5/6}\, \gamma \sqrt{S_t m^*} V_t^{rel} \tag{33}$$

δ_t is the tangential overlap, S_t is the tangential stiffness and G^* is the equivalent shear modulus. V_t^{rel} denotes the tangential component of the relative velocity between two particles.

The tangential force is limited by the Coulomb friction ($\mu_s F_n$) where μ_s represents the limiting friction coefficient. If the net tangential force reaches the frictional force then sliding occurs. The rolling friction is accounted for by applying a torque to the contacting surfaces which is a function of normal force F_n and coefficient of rolling friction μ_r [48].

$$\tau_{r,i} = -\mu_r F_n R_i \omega_i \tag{34}$$

5. **Set-up of Simulation for Pneumatic Conveying**

A 2.15 m length of the pneumatic conveying line is simulated in a 3D geometry. The computational domain is discretized to tetrahedral grids which are 3 to 8 times of the particle size. The domain was divided into 205,490 tetrahedral mesh elements, with 397,376 nodes [18]. This mesh size was found to produce accurate results and reasonably fast simulation. Gas and particle flow rates in the simulations were matched with the experiments. Particles were created in the inclined pipe with an initial velocity u_x= 0.0635 m/s to replicate the screw feeder in the experiments. A time step equal to 30% of Rayleigh time is chosen for the DEM time step and the Eulerian time step was set to 100 times this. All parameters used in the pneumatic conveying simulation of spherical and non-spherical particles in FLUENT-EDEM are summarized in Table 3. the $C_{\varepsilon 3}$ value is selected equal to 1.7 in equation (17) according to the calibration performed in our previous study [32]. A snapshot of the experiment in comparison with the simulation is seen in Figure 2.

Non-spherical particles in EDEM software are approximated using the overlapping spherical particles which are fixed in position relative to each other along the major axis of symmetry, as can be seen in Figure. 3. The centre of mass and particle moment of inertia are calculated by the EDEM software [46].

The contact search, contact detection and calculation of force are the same as those explained for single sphere particles. The contact detection between two multi-sphere particles is based on detection of contacts between their element spheres. The contact forces on elements are transferred to the centroid of the particle to which they belong ([49] and [50]). A comprehensive explanation about the calculation of the resultant force and momentum acting

on each multi-sphere particle element and non-spherical particle due to particle-particle or particle-geometry contacts can be found in [50].

6. Results and Discussion for Spherical Particles

6.1. Comparison between Simulation and Experiments for Mean Axial Particle Velocity

Prior to comparing the experiment and the simulation, the influence of the drag force model on the particle velocity was investigated because the drag force is the dominant force in pneumatic conveying which controls the particle velocity. Two widely used drag models from Ergun and Wen & Yu ([34] and [35]) and Di Felice [36] were applied.

In the experiments, particle velocity was measured for 15 points of a cross section in the horizontal direction and 15 points of a cross section in the vertical direction. Therefore, in the simulation post processing, the corresponding conveying line cross section was divided into 15 “grid bins” in the horizontal direction and 15 grid bins in the vertical direction such that each of these grid bins has 5 mm side length and represents a measurement point in the experiment. When a particle is passing through a specific grid bin, the particle velocity is computed for that grid bin and at the end of the simulation time a temporally averaged velocity is obtained for all the particles which passed through the specific grid bin. This temporally averaged velocity then is compared with the experimentally measured particle velocity.

The experimental results of horizontal and vertical profiles of particle velocity, the simulation results with Ergun and Wen & Yu drag models, and the simulation results with Di Felice drag model are presented in Figure. 4 to Figure. 7 for 2 mm glass beads with SLR=2.3 and 3.0 at

z=1 m. In all cases, it is clearly observed that the Di Felice drag model predicts a higher particle velocity than the Ergun and Wen & Yu drag model, which means the discrepancy between experimental and simulation results increases considerably by using the Di Felice drag model compared to that of Ergun and Wen & Yu.

Numerous correlations for calculating the drag coefficient of gas–solid systems have been reported in literature, including [51-53], all of which can be implemented into the FLUENT-EDEM code. However, even if a drag model giving more accurate results can be found for this study, it would not be possible to conclude the appropriateness of the drag model in other pneumatic conveying simulations with different particle sizes and flow regimes; further an investigation of drag modelling, which has been widely discussed in the past [54] was not an aim of this study. We decided to adopt the Ergun and Wen & Yu drag model which produced the better prediction for spherical particles (see Figures 4-7). The possible reasons for the discrepancies observed between the experiment and simulation results are discussed in detail in section 6.1.1.

As it is seen in Figure. 4 and Figure. 6, for the horizontal profiles, similar to the experimental results, a relatively flat mean particle velocity profile is obtained in the central parts of the pipe. However, the particle velocity decrease close to the pipe wall is not seen in the simulation results and obviously, the model is not capable of predicting the particle velocity close to the pipe wall. The discrepancy between experimental and simulation results increases for the measurement points closer to the pipe wall. In the CFD-DEM model, the mesh size needs to be larger than the particle size [13]. Therefore, the fluid flow is not resolved well close to the walls. This issue decreases the accuracy of the fluid flow calculation in these regions and is a feature of CFD-DEM calculations. The average relative discrepancies

between simulation and experiment for 2 mm glass beads, SLR=2.3 and 2 mm glass beads, SLR=3 in the central region of the pipe are of the order of 22% and 35% respectively.

As seen in the vertical profile of particle velocity, Figure. 5 and Figure. 7, the particle velocity increases from the lower section of the pipe and reaches a maximum point in the upper section of the pipe before decreasing toward the upper pipe wall. This behaviour is also observed in the experimental results. However, the model cannot capture the noticeable particle velocity decrease close to the pipe wall accurately due to fluid meshing constraints, just discussed. The average relative discrepancy of 25%, for 2 mm glass beads, SLR=2.3 and around 35%, for 2 mm glass beads, SLR=3, is seen for the vertical profiles.

In summary, our CFD-DEM simulations have consistently over-predicted the particle velocity in both the horizontal and the vertical profiles. However, the general particle velocity trend is broadly captured except for the near-wall regions.

The numerical and experimental results for the smaller glass beads of 1.5 mm are compared in Figure. 8 and Figure. 9. For SLR cases of 2.3, 3.0 and 3.5. Similar to the 2 mm glass beads, a flat mean particle velocity profile is obtained for the horizontal profile. In the vertical profile, particle velocity is smaller in the lower section of the pipe, it increases to a maximum value and decreases slightly again toward the upper pipe wall. The velocity decrease close to the pipe walls observed in the experimental results is not seen in the simulation results as was the case for the larger spherical glass beads,

The numerically computed particle velocity is over-predicting the experimental measurement. For 1.5 mm particle, the average relative discrepancy for SLR=2.3 case is 25% in the

horizontal and vertical profiles as compared with average discrepancies of 33%-38% for the SLR=3.0 case. Figure. 8 and Figure. 9 show that when SLR increases further to 3.5, the average discrepancy in the horizontal profile is around 55% and for the vertical profile it is around 36%.

Figure.10 and Figure.11 show the horizontal and vertical profiles of the mean axial particle velocity for 0.8-1 mm particles with SLR=2.3. Similar to 1.5 mm and 2 mm particles, the particle velocity is relatively constant for the horizontal profile but increases noticeably from the lower section of the pipe toward the upper part of the pipe in the vertical profile. The average relative discrepancies between experimental and simulation results are around 40% and 36% for the horizontal and vertical profiles respectively.

6.1.1 **Sources of discrepancies between simulation and experiments**

As observed in all figures in this section, the numerically predicted particle velocity over-predicted the experimental results. A likely reason for the over-estimation of the particle velocity is the inaccurate prediction of drag force. Drag model correlations should be employed with caution as they are usually derived for an isolated single particle and for a specific flow condition, and then corrected to take into account the effect of neighbouring particles in a bulk suspension. For instance, the Di Felice [36] drag model was derived for particle sedimentation, whilst the Ergun [34] drag correlation was derived based on the empirical correlations for pressure drop in a packed bed. However, these drag coefficients cannot be used universally for all flow conditions, and there is no general agreement about the modelling of gas-particle drag [55] and [56]. This shows that more research needs to be performed in this field. Such research is however beyond the scope of our research.

A further consideration regarding the discrepancy between experiment and simulation is that in CFD-DEM, the fluid velocity at the particle location needs to be determined from the CFD grid information to calculate the relative velocity and drag force. However, in the coupled FLUENT-EDEM, fluid velocity is not interpolated to the particle location, and all particles in a mesh experience the same fluid velocity regardless of the particle position within the fluid mesh cell. Interpolation methods suggested by Xiao and Sun [57], Sommerfeld et al. [58] or Elghobashi [59] could, given time, be implemented in the FLUENT-EDEM code.

6.2. Comparison between Simulation and Experiments for mean axial Gas Velocity

Figure. 12 shows the horizontal profile of the simulated and measured mean gas velocity in the presence of 1.5 mm spherical particles at SLR=2.3, 3 and 3.5. The simulation predicts a relatively flat mean gas velocity profile (in the central parts of the pipe) for the particle laden flow compared to the parabolic profile for the mean gas velocity of clear gas flow. This trend is also seen in the experimental results. Simulation results are qualitatively in agreement with the experimental results but with a consistent over-prediction.

The corresponding vertical profiles of mean gas velocity in the presence of 1.5 mm glass beads at SLR=2.3, 3 and 3.5 is shown in Figure.13. Both experimental and simulation results show that the maximum gas velocity shifted upward from the pipe centre because the flow resistance due to particles is lower in the pipe upper section where a lesser number of particles were transported. Correspondingly, the gas velocity decreased in the lower section of the pipe, where a high number of particles were conveyed due to gravity. This trend also was observed by Tsuji and Morikawa [11].

The mean gas velocity in vertical profile was again predicted to be higher than the experiments at all measurement points, but with less discrepancy than for the horizontal profiles.

Figure. 14 to Figure. 17 present the comparison between simulation and experimental results of horizontal and vertical profiles of mean gas velocity in the presence of 2 mm glass beads with SLR=2.3 and 3.0 and 0.8-1 mm glass beads with SLR=2.3. Similar trends to the mean gas velocity as described above for the case of 1.5 mm glass beads were observed in all these graphs, including the consistent over prediction of the numerical results.

In summary, the numerical model predicted the gas velocity profiles which are in good qualitative agreement with the experiments but significantly over-predicted the magnitude. It seems that the model has not captured the effect of particles on the gas profile accurately, which can be attributed to the fluid discretization. As mentioned previously, the fluid mesh has to be larger than the particle scale to improve statistical averaging. The size of the computational cells may not be small enough to replicate the fluid pattern accurately.

7. **Pneumatic Transportation of Low-Aspect-Ratio Cylindrical Particles**

Cylindrical particles with low-aspect-ratio (defined as a ratio of particle length to the particle diameter) were pneumatically conveyed in the same experimental setup with the horizontal profiles of particle velocity were measured at two cross-sections z=1 m and z=2 m. The particle characteristics and experimental conditions are summarized in Table 4.

Experiments were carried out for three different SLRs at 0.6, 1.0 and 1.2. The horizontal profiles of mean axial particle velocity are shown in Figure. 18 and Figure.19. A flat

horizontal profile for mean axial particle velocity is predicted as was previously seen for spherical particles. It is also seen that by increasing the SLR, the mean axial particle velocity decreases.

The simulations are compared with the experiments in Figure. 20 and Figure.21. The mean axial particle velocities are under-predicted in the simulations. Mean relative discrepancies of 20% and 25% are observed for SLR=0.6 and SLR=1 respectively for the simulations implementing the Ganser [39] drag coefficient model. The relative discrepancy is 18% and 20% for the simulations with the drag coefficient model proposed by Haider and Levenspiel [38] for SLR=0.6 and SLR=1 respectively.

Hölzer and Sommerfeld [60] considered a large number of experimental data (665 values) for isometric particles in the Stokes region. They reported the mean relative errors between experimental values and the correlation formulas of Ganser [39] and Haider and Levenspiel [38] were around 6.46% and 6.65% respectively. Obviously applying the C_D model proposed by Ganser [39] and Haider and Levenspiel[38] for a turbulent dynamic system such as pneumatic conveying can increase the relative error between experiment and simulation, because these drag coefficients have not been derived for such conditions.

8. **Discussion: Predictive Capability**

A summary of the predictive capability of the CFD-DEM simulations for the various cases studies is included in Table 5.

As seen, a relative discrepancy range from 22 % to 55% is observed when the simulation results are compared with the experimental results for particle laden flow in the presence of spherical particles. This relative discrepancy is from 18% to 25% for pneumatic transportation of non-spherical particles. It may be concluded that the CFD-DEM model is not capable of predicting the experimental results precisely. However, all the assumptions and limitations discussed in section 6.1.1 regarding the drag models, computational domain mesh size and also the lack of interpolation scheme in the coupled FLUENT and EDEM must be born in mind. Despite the quantitative inaccuracy, we believe the CFD-DEM implemented model can provide relatively useful qualitative results provided the user interprets them with extreme care.

9. **Conclusions**

A study was performed to evaluate the capabilities of the CFD-DEM approach as a tool in the modelling of horizontal pneumatic conveying. A series of experimental measurements with the aid of laser Doppler anemometry (LDA) were conducted to measure gas and particle velocities at different locations in the conveying line for both horizontal and vertical directions. Spherical and low-aspect-ratio non-spherical particles were used.

Simulations were carried out using a coupled CFD-DEM approach by means of the EDEM and FLUENT commercial softwares with API coded add-ons for more complex functions including drag and carrier-phase turbulence modulation.

It was concluded that CFD-DEM approach could qualitatively capture some of the features of the horizontal pneumatic conveying observed experimentally. However a relative discrepancy ranged from 22% to 55% was observed for particle laden flows in the presence

of spherical particles for different SLRs and particle sizes. The computational model consistently over-predicted the mean gas velocity when compared with the experimental measurements. This discrepancy could be attributed to the mesh size which needs to be several times larger than the particle size in the CFD-DEM approach.

The mean particle velocity was also over-predicted compared with the experiments. This deviation was explained due to the inexact computation of the drag force. The lack of a scheme in the coupled FLUENT-EDEM code to interpolate the gas velocity at the grid locations onto the precise particle position to calculate the drag force could be another source of error.

A relative discrepancy between CFD-DEM simulation and experiment of 18% to 25% for pneumatic conveying of non-spherical particles was observed. In the simulation; the influence of particle orientation on aerodynamic forces and torque was ignored. The discrepancy observed between experimental and simulation results for the horizontal profile of mean axial particle velocity was explained due to the implemented drag models in the simulations.

According to our results, it can be concluded that CFD-DEM can qualitatively predict the phenomena happening in a horizontal pneumatic conveying system. However, special attention needs to be paid regarding assumptions and simplification associated with this method, such as selection of the appropriate drag model, mesh size and interpolation scheme.

The detailed experimental data obtained in this study along with the experimental parameters is available to the research community for future validation work on horizontal pneumatic conveying.

Acknowledgment

This work has been carried out as a part of the PARDEM project, an EU-funded, Framework 7 Marie Curie Initial Training Network. The financial support provided by the European Commission is gratefully acknowledged.

REFERENCES

[1] M. Sommerfeld, N. Huber, Experimental analysis and modelling of particle-wall collisions, International Journal of Multiphase Flow, 25 (1999) 1457-1489.

[2] J.R. Kadambi, W.T. Martin, S. Amirthaganesh, M.P. Wernet, Particle sizing using particle imaging velocimetry for two-phase flows, Powder Technology, 100 (1998) 251-259.

[3] H. Li, Y. Tomita, Particle velocity and concentration characteristics in a horizontal dilute swirling flow pneumatic conveying, Powder Technology, 107 (2000) 144-152.

[4] G.R. Caicedo, J.J.P. Marqués, M.G.a. Ruíz, J.G. Soler, A study on the behaviour of bubbles of a 2D gas–solid fluidized bed using digital image analysis, Chemical Engineering and Processing: Process Intensification, 42 (2003) 9-14.

[5] R.E. van de Wall, S.L. Soo, Measurement of particle cloud density and velocity using laser devices, Powder Technology, 81 (1994) 269-278.

[6] K.L. Ostrowski, S.P. Luke, M.A. Bennett, R.A. Williams, Application of capacitance electrical tomography for on-line and off-line analysis of flow pattern in horizontal pipeline of pneumatic conveyer, Chemical Engineering Journal, 77 (2000) 43-50.

[7] B.J. Azzopardi, K. Jackson, J.P. Robinson, R. Kaji, M. Byars, A. Hunt, Fluctuations in dense phase pneumatic conveying of pulverised coal measured using electrical capacitance tomography, Chemical Engineering Science, 63 (2008) 2548-2558.

[8] S.L. Lee, F. Durst, On the motion of particles in turbulent duct flows, International Journal of Multiphase Flow, 8 (1982) 125-146.

[9] S. Frank, C. Heilmann, H.E. Siekmann, Point-velocity methods for flow-rate measurements in asymmetric pipe flow, Flow Measurement and Instrumentation, 7 (1996) 201-209.

[10] D. Roy, F. Larachi, R. Legros, J. Chaouki, A study of solid behavior in spouted beds using 3-D particle tracking, The Canadian Journal of Chemical Engineering, 72 (1994) 945-952.

[11] S. Laín, M. Sommerfeld, J. Kussin, Experimental studies and modelling of four-way coupling in particle-laden horizontal channel flow, International Journal of Heat and Fluid Flow, 23 (2002) 647-656.

[12] S. Laín, M. Sommerfeld, Euler/Lagrange computations of pneumatic conveying in a horizontal channel with different wall roughness, Powder Technology, 184 (2008) 76-88.

[13] Y. Lu, An Investigation of the particle dynamics of a multi-component solid phase in a dilute phase pneumatic conveying system, *Ph.D. Thesis*, The University of Edinburgh, 2009.

[14] Y. Tsuji, Y. Morikawa, LDV measurements of an air-solid two-phase flow in a horizontal pipe, Journal of Fluid Mechanics, 120 (1982) 385-409.

[15] U. Datta, T. Dyakowski, S. Mylvaganam, Estimation of particulate velocity components in pneumatic transport using pixel based correlation with dual plane ECT, Chemical Engineering Journal, 130 (2007) 87-99.

[16] Y. Tsuji, T. Tanaka, T. Ishida, Lagrangian numerical simulation of plug flow of cohesionless particles in a horizontal pipe, Powder Technology, 71 (1992) 239-250.

[17] C.K.K. Lun, H.S. Liu, Numerical simulation of dilute turbulent gas-solid flows in horizontal channels, International Journal of Multiphase Flow, 23 (1997) 575-605.

[18] F.Y. Fraige, P.A. Langston, Horizontal pneumatic conveying: a 3d distinct element model, Granular Matter, 8 (2006) 67-80.

[19] S.B. Kuang, A.B. Yu, Micromechanic modeling and analysis of the flow regimes in horizontal pneumatic conveying, AIChE Journal, 57 (2011) 2708-2725.

[20] C.K.K. Lun, Numerical simulation of dilute turbulent gas-solid flows, International Journal of Multiphase Flow, 26 (2000) 1707-1736.

[21] Y. Tsuji, Y. Morikawa, H. Shimoni, LDV measurements of an air-solid two-phase flow in a vertical pipe, Journal of Fluid Mechanics, 139 (1984) 417-434.

[22] R. Clift, W.H. Gauvin, Motion of entrained particles in gas streams, The Canadian Journal of Chemical Engineering, 49 (1971) 439-448.
[23] M. Sommerfeld, Validation of a stochastic Lagrangian modelling approach for inter-particle collisions in homogeneous isotropic turbulence, International Journal of Multiphase Flow, 27 (2001) 1829-1858.
[24] H. Zhang, G. Ahmadi, F.-G. Fan, J.B. McLaughlin, Ellipsoidal particles transport and deposition in turbulent channel flows, International Journal of Multiphase Flow, 27 (2001) 971-1009.
[25] L. Rosendahl, Using a multi-parameter particle shape description to predict the motion of non-spherical particle shapes in swirling flow, Applied Mathematical Modelling, 24 (2000) 11-25.
[26] J.E. Hilton, P.W. Cleary, The role of particle shape in pneumatic conveying, Seventh International Conference of CFD in the Minerals and Process IndustriesMelbourne, Australia, 2009, pp. 1-6.
[27] S. Laín, M. Sommerfeld, A study of the pneumatic conveying of non-spherical particles in a turbulent horizontal channel flow, Brazilian Journal of Chemical Engineering, 24 (2007) 535-546.
[28] J.E. Hilton, P.W. Cleary, The influence of particle shape on flow modes in pneumatic conveying, Chemical Engineering Science, 66 (2012) 231-240.
[29] J. Lin, X. Shi, Z. Yu, The motion of fibers in an evolving mixing layer, International Journal of Multiphase Flow, 29 (2003) 1355-1372.
[30] M. Mandø, C. Yin, H. Sørensen, L. Rosendahl, On the modelling of motion of non-spherical particles in two-phase flow, 6th international conference on multiphase flow (ICMF)Leipzig, Germany, 2007.
[31] A. Doukelis, M. Founti, K. Mathioudakis, K. Papailiou, Evaluation of beam refraction effects in a 3D laser Doppler anemometry system for turbomachinery applications, Measurement Science and Technology, 7 (1996) 922.
[32] M. Ebrahimi, CFD-DEM modelling of two-phase pneumatic conveying with experimental validation, The University of Edinburgh, 2014.
[33] T.B. Anderson, R. Jackson, Fluid Mechanical Description of Fluidized Beds. Equations of Motion, Industrial & Engineering Chemistry Fundamentals, 6 (1967) 527-539.
[34] S. Ergun, Fluid Flow Through Packed column, Chemical Engineering progress, 48 (1952) 89-94.
[35] C.Y. Wen, Y.H. Yu, Mechanics of Fluidisation, Chemical Engineering Progress Symposium Series, 62 (1966) 100-111.
[36] R. Di Felice, The voidage function for fluid-particle interaction systems, International Journal of Multiphase Flow, 20 (1994) 153-159.
[37] J.E. Hilton, P.W. Cleary, The influence of particle shape on flow modes in pneumatic conveying, Chemical Engineering Science, 66 (2011) 231-240.
[38] A. Haider, O. Levenspiel, Drag coefficient and terminal velocity of spherical and nonspherical particles, Powder Technology, 58 (1989) 63-70.
[39] G.H. Ganser, A rational approach to drag prediction of spherical and nonspherical particles, Powder Technology, 77 (1993) 143-152.
[40] M. Ebrahimi, M. Crapper, J.Y. Ooi, Experimental and Simulation Studies of Dilute Horizontal Pneumatic Conveying, Particulate Science and Technology, 32 (2014) 206-213.
[41] B. Oesterlé, T.B. Dinh, Experiments on the lift of a spinning sphere in a range of intermediate Reynolds numbers, Experiments in Fluids, 25 (1998) 16-22.
[42] B.E. Launder, D.B. Spalding, Lectures in Mathematical Models of Turbulence, Academic Press, London, England, (1972).
[43] S. Geiss, A. Dreizler, Z. Stojanovic, M. Chrigui, A. Sadiki, J. Janicka, Investigation of turbulence modification in a non-reactive two-phase flow, Experiments in Fluids, 36 (2004) 344-354.
[44] M. Mandø, Turbulence modulation by non-spherical particles, Department of energy technology, Aalborg University, (2009).
[45] Y. Zhang, J.M. Reese, Gas turbulence modulation in a two-fluid model for gas–solid flows, AIChE Journal, 49 (2003) 3048-3065.

[46] DEMSolutions Ltd, EDEM-CFD coupling for FLUENT, User guide, (2010).
[47] R.D. Mindlin, H. Deresiewicz, Elastic spheres in contact under varying oblique forces, Journal of applied mechanics, 21 (1953) 327-344.
[48] J. Ai, J.-F. Chen, J.M. Rotter, J.Y. Ooi, Assessment of rolling resistance models in discrete element simulations, Powder Technology, 206 (2011) 269-282.
[49] J.F. Favier, M.H. Abbaspour-Fard, M. Kremmer, A.O. Raji, Shape representation of axi-symmetrical, non-spherical particles in discrete element simulation using multi-element model particles, Engineering computations 16 (1999) 467-480.
[50] M.H. Abbaspour-Fard, Discrete element modelling of the dynamic behaviour of non-spherical particulate materials, *Ph.D. Thesis*, Newcastle University, 2000, pp. Newcastle University.
[51] M. Syamlal, T.J. O'brien, Computer simulation of bubbles in a fluidized bed, AIChE Symp. Ser, 85 (1989) 22-31.
[52] D. Gidaspow, Multiphase flow and fluidization: continuum and kinetic theory descriptions, Academic press1994.
[53] R. Beetstra, M.A. Van der Hoef, J.A.M. Kuipers, Drag force of intermediate Reynolds number flow past mono‐ and bidisperse arrays of spheres, AIChE journal, 53 (2007) 489-501.
[54] N.G. Deen, M. Van Sint Annaland, M.A. Van der Hoef, J.A.M. Kuipers, Review of discrete particle modeling of fluidized beds, Chemical Engineering Science, 62 (2007) 28-44.
[55] M.J.V. Goldschmidt, R. Beetstra, J.A.M. Kuipers, Hydrodynamic modelling of dense gas-fluidised beds: comparison and validation of 3D discrete particle and continuum models, Powder Technology, 142 (2004) 23-47.
[56] M. Sturm, S. Wirtz, V. Scherer, J. Denecke, Coupled DEM-CFD Simulation of Pneumatically Conveyed Granular Media, Chemical Engineering & Technology, 33 (2010) 1184-1192.
[57] H. Xiao, J. Sun, Algorithms in a Robust Hybrid CFD-DEM Solver for Particle-Laden Flows, Communications in Computational Physics, 9 (2011) 297.
[58] M. Sommerfeld, G. Kohnen, M. Rüger, Some open questions and inconsistencies of Lagrangian particle dispersion models, Ninth symposium on "turbulent shear flows"Kyoto, Japan, 1993.
[59] S. Elghobashi, On predicting particle-laden turbulent flows, Applied Scientific Research, 52 (1994) 309-329.
[60] A. Hölzer, M. Sommerfeld, New simple correlation formula for the drag coefficient of non-spherical particles, Powder Technology, 184 (2008) 361-365.

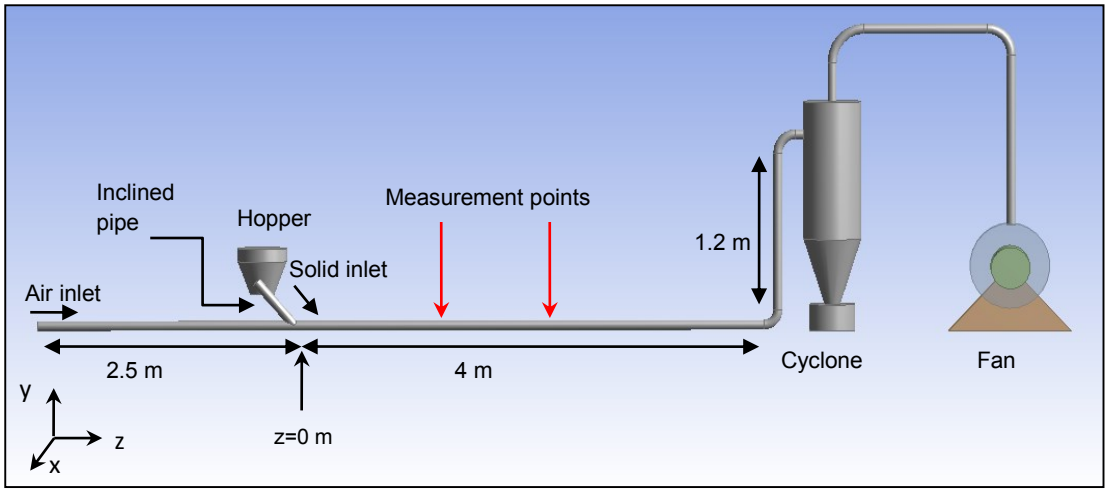

Figure. 1: Schematic of pneumatic conveying system.

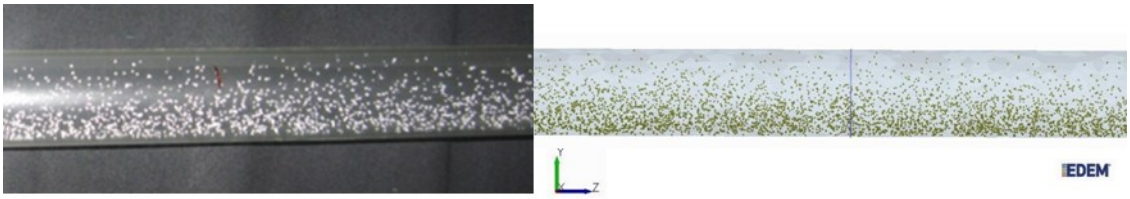

(a) **(b)**

Figure. 2: Experiment snapshot (a) in comparison with the simulation (b). 1.5 mm glass beads, SLR=2.3

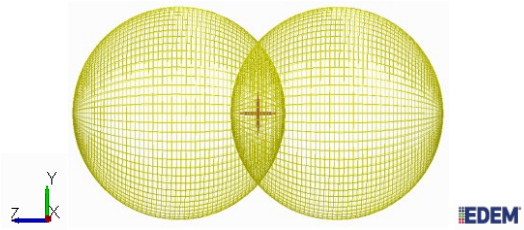

Figure. 3: Representation of a non-spherical particle in EDEM.

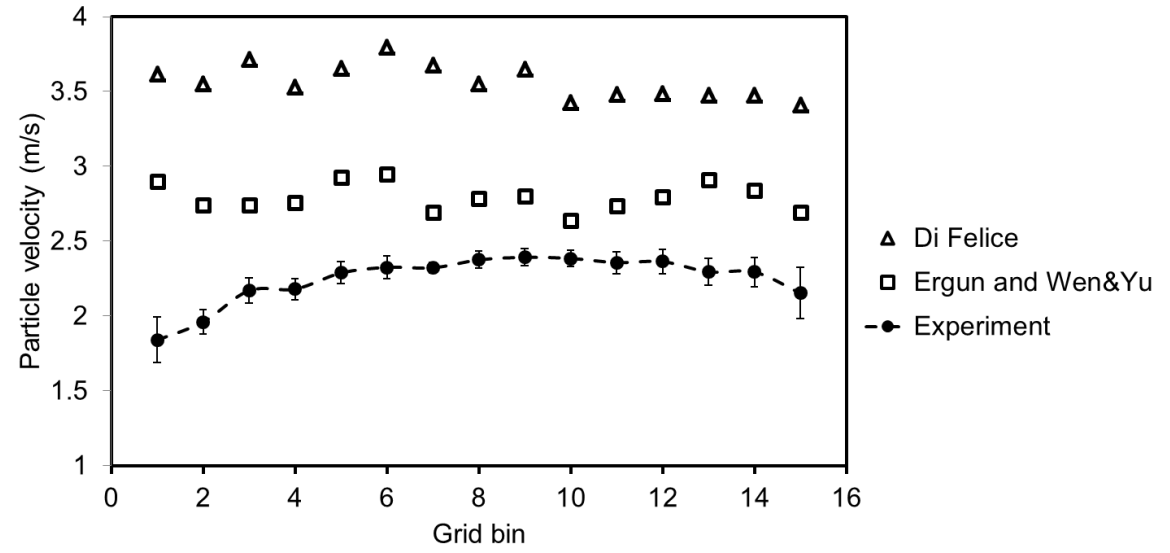

Figure. 4: Effect of the drag model on the horizontal profile of particle velocity, 2 mm glass beads, SLR=2.3, z=1 m.

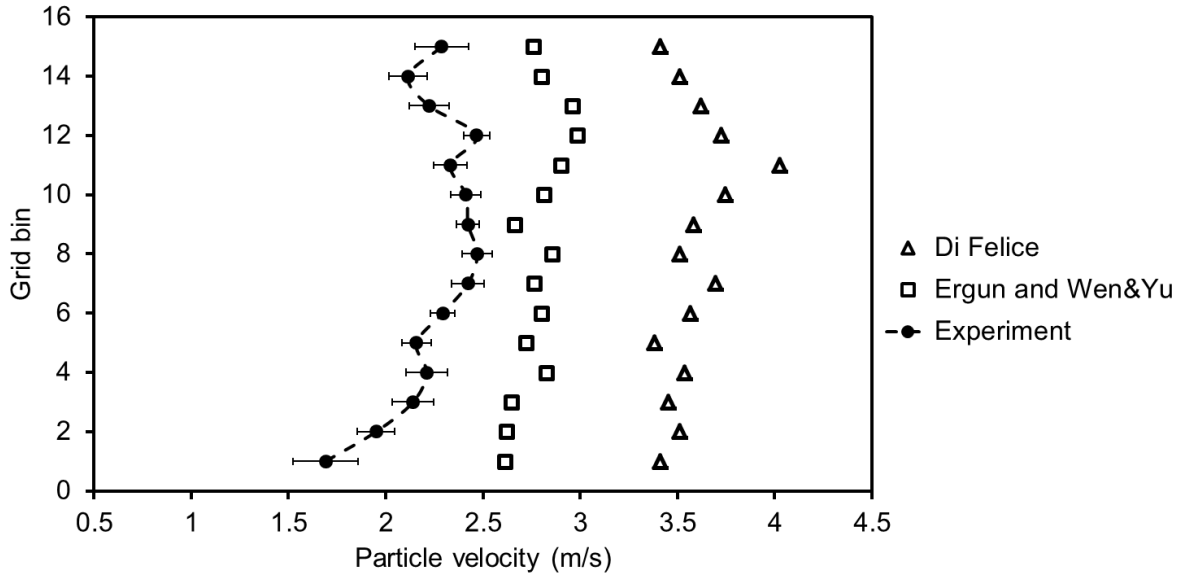

Figure. 5: Effect of the drag model on the vertical profile of particle velocity, 2 mm glass beads, SLR=2.3, z=1 m**.**

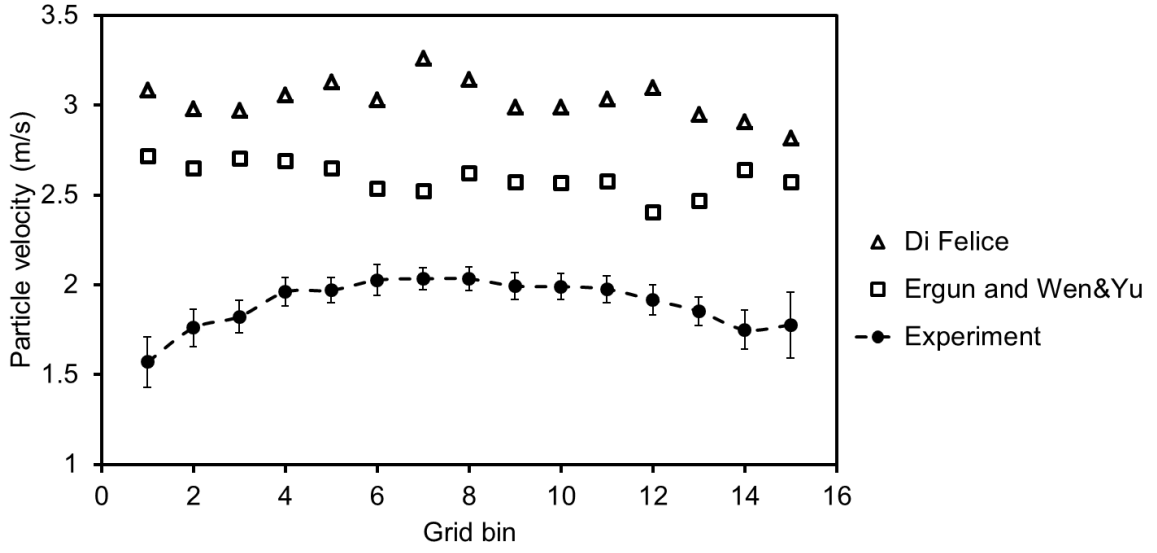

Figure. 6: Effect of the drag model on the horizontal profile of particle velocity, 2 mm glass beads, SLR=3, z=1 m.

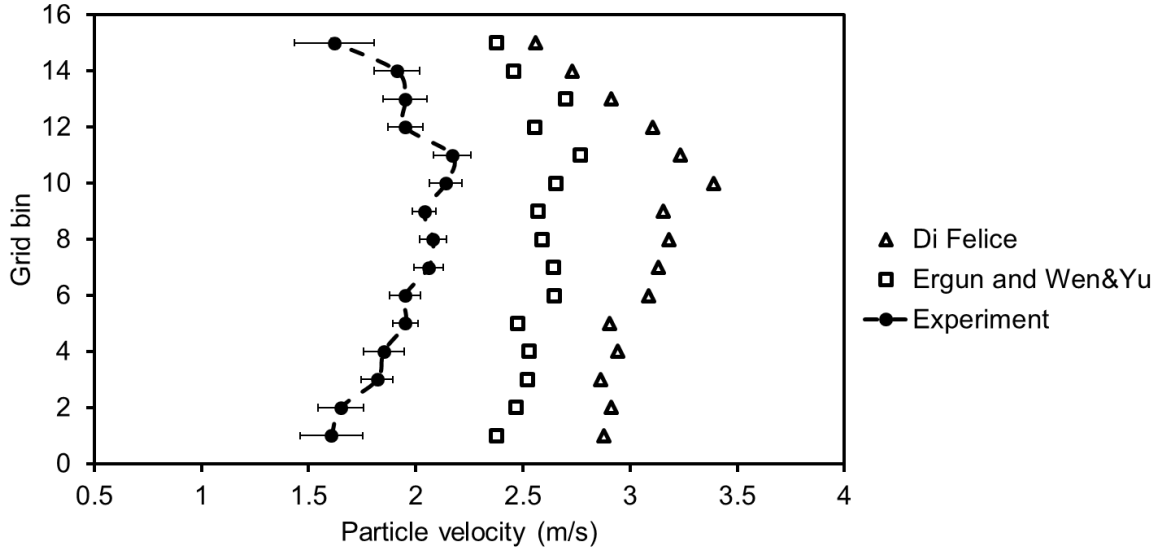

Figure. 7: Effect of the drag model on the vertical profile of particle velocity, 2 mm glass beads, SLR=3, z=1 m.

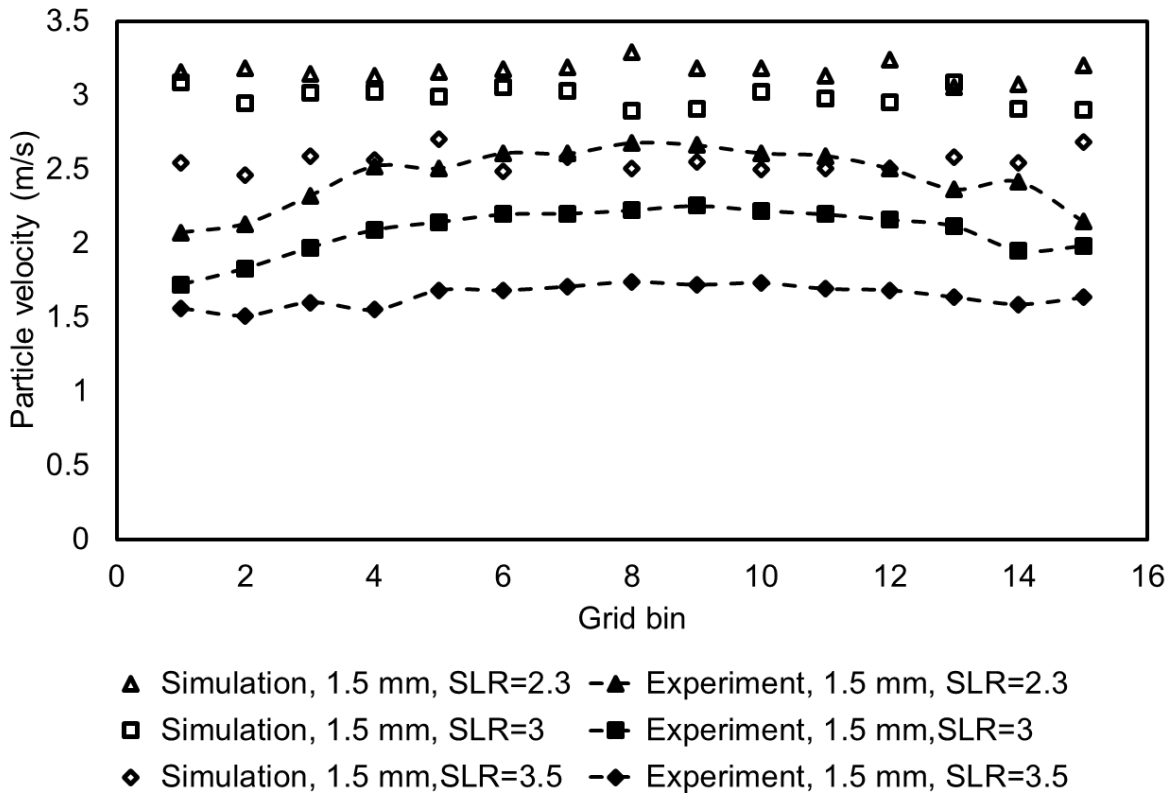

Figure. 8: Particle velocity comparison between experiment and simulation for horizontal profile of 1.5 mm glass beads, SLR=2.3, 3, 3.5, z=1 m.

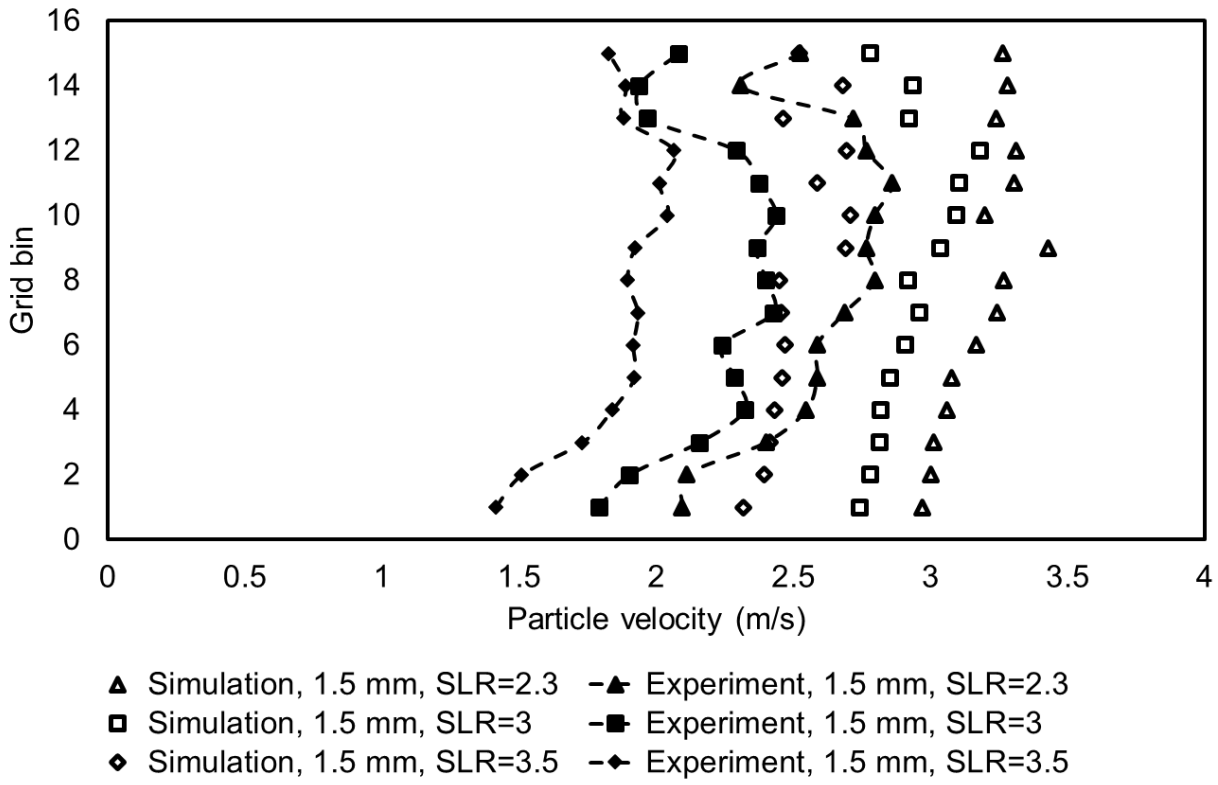

Figure. 9: Particle velocity comparison between experiment and simulation for vertical profile of 1.5 mm glass beads, SLR=2.3, 3, 3.5, z=1 m.

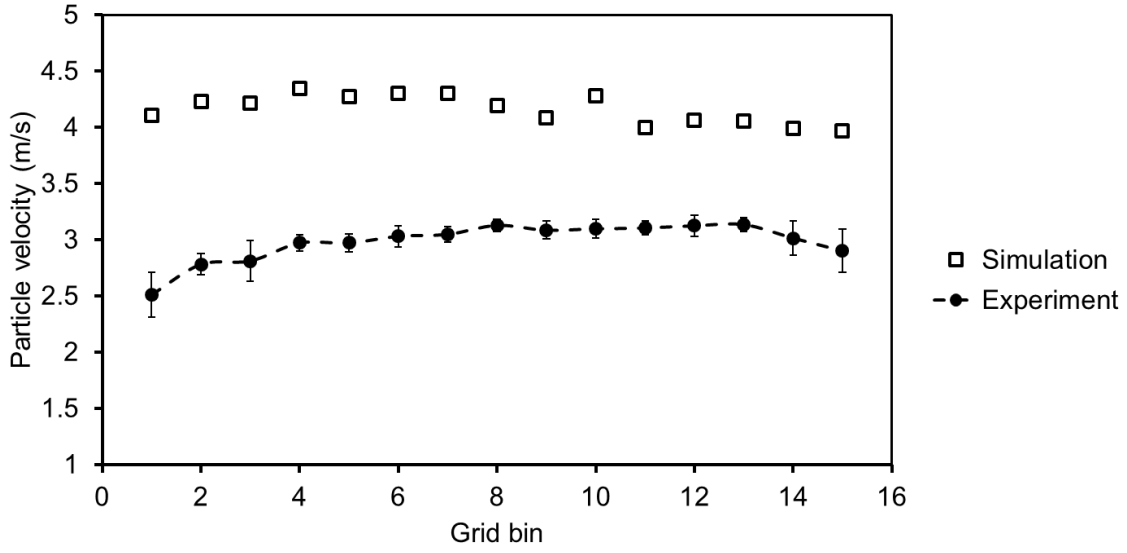

Figure. 10: Particle velocity comparison between simulation and experiment for horizontal profile in the presence of 0.8-1 mm glass beads, z=1 m, SLR=2.3.

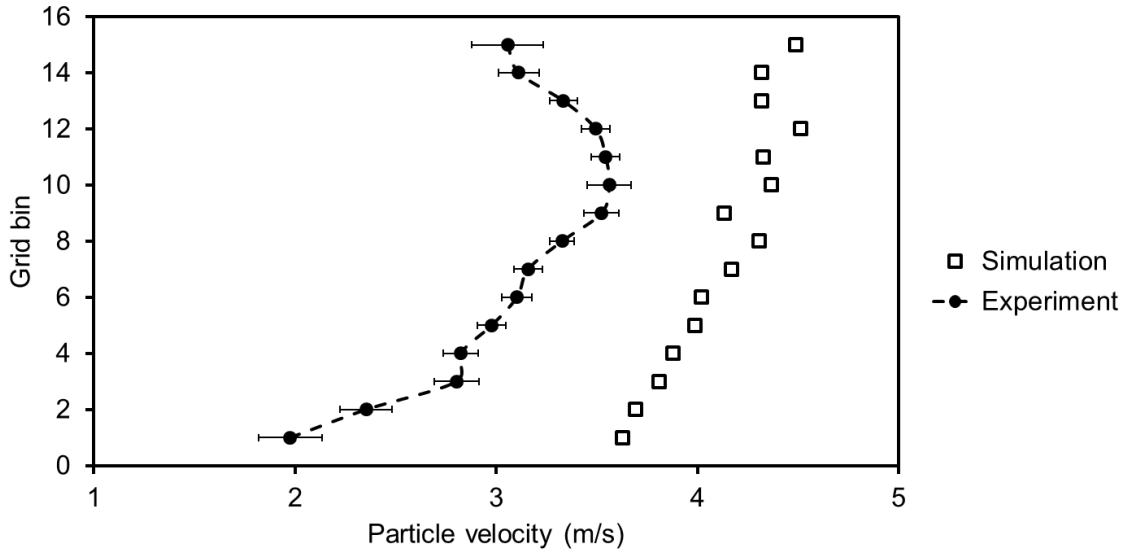

Figure. 11: Particle velocity comparison between simulation and experiment for vertical profile in the presence of 0.8-1 mm glass beads, z=1 m, SLR=2.3.

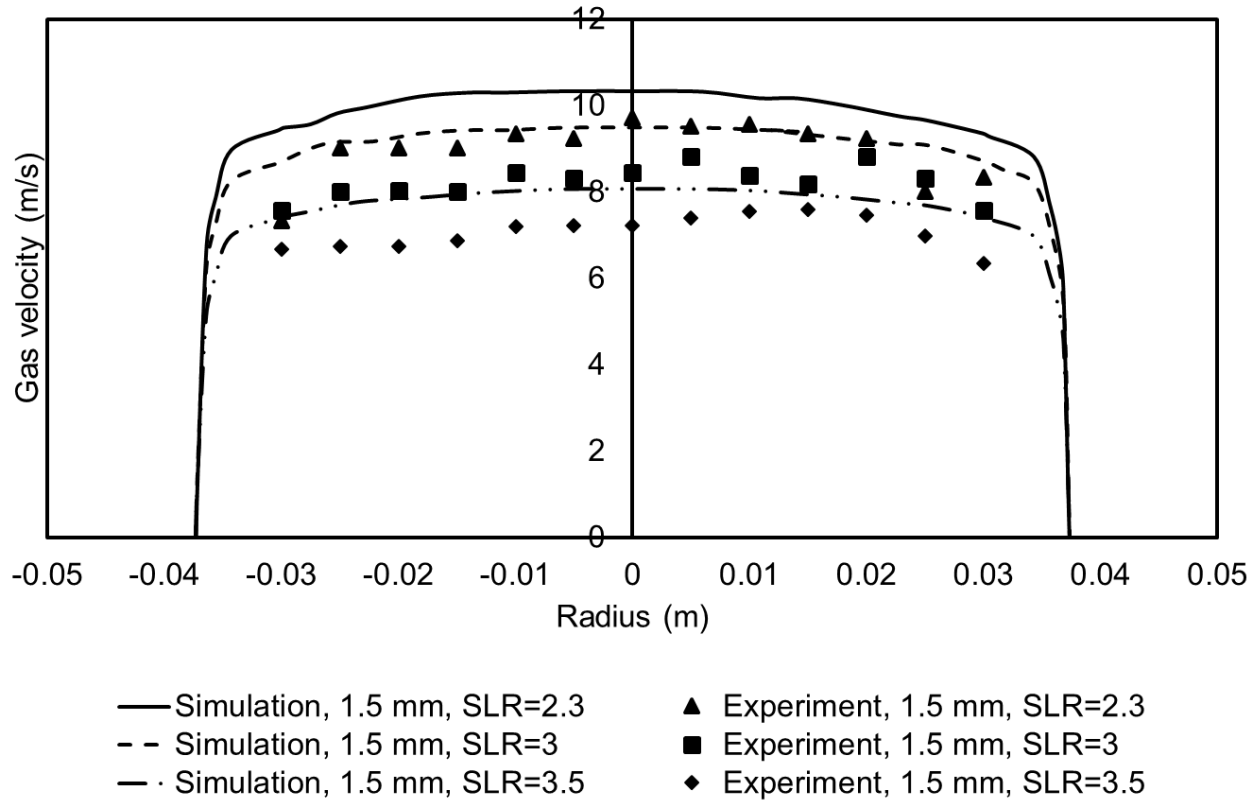

Figure. 12: Gas velocity comparison between simulation and experiment for horizontal profile in the presence of 1.5 mm glass beads, SLR=2.3, 3, 3.5, z=2 m.

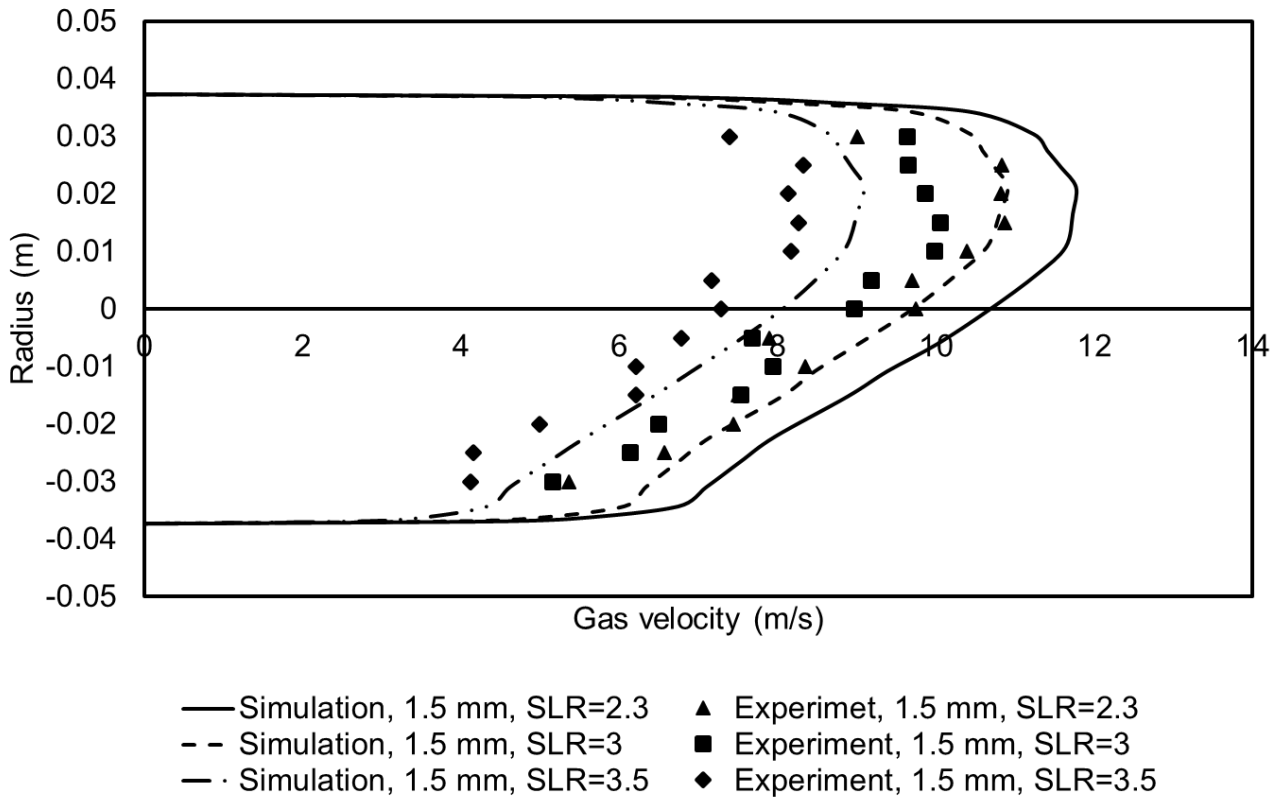

Figure. 13: Gas velocity comparison between simulation and experiment for vertical profile in the presence of 1.5 mm glass beads, SLR=2.3, 3, 3.5, z=2 m.

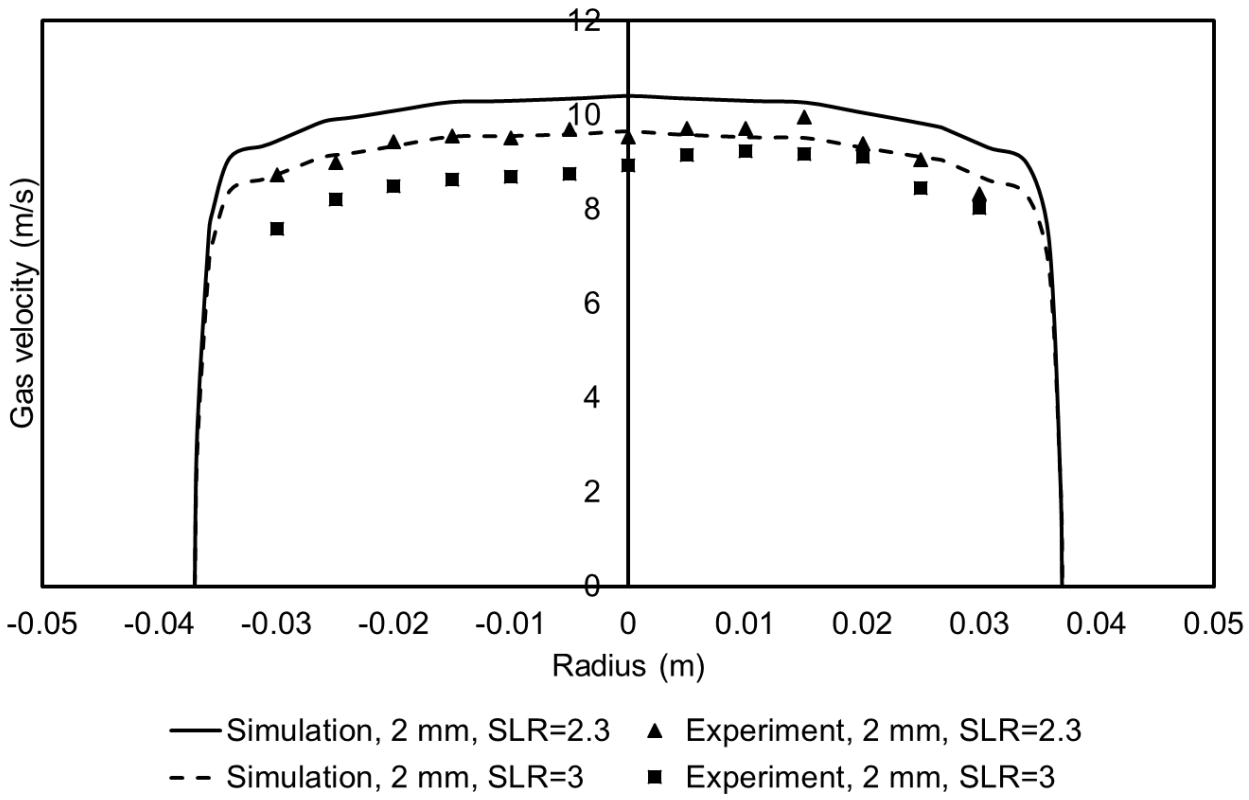

Figure. 14: Gas velocity comparison between simulation and experiment for horizontal profile in the presence of 2 mm glass beads, SLR=2.3, 3, z=2 m.

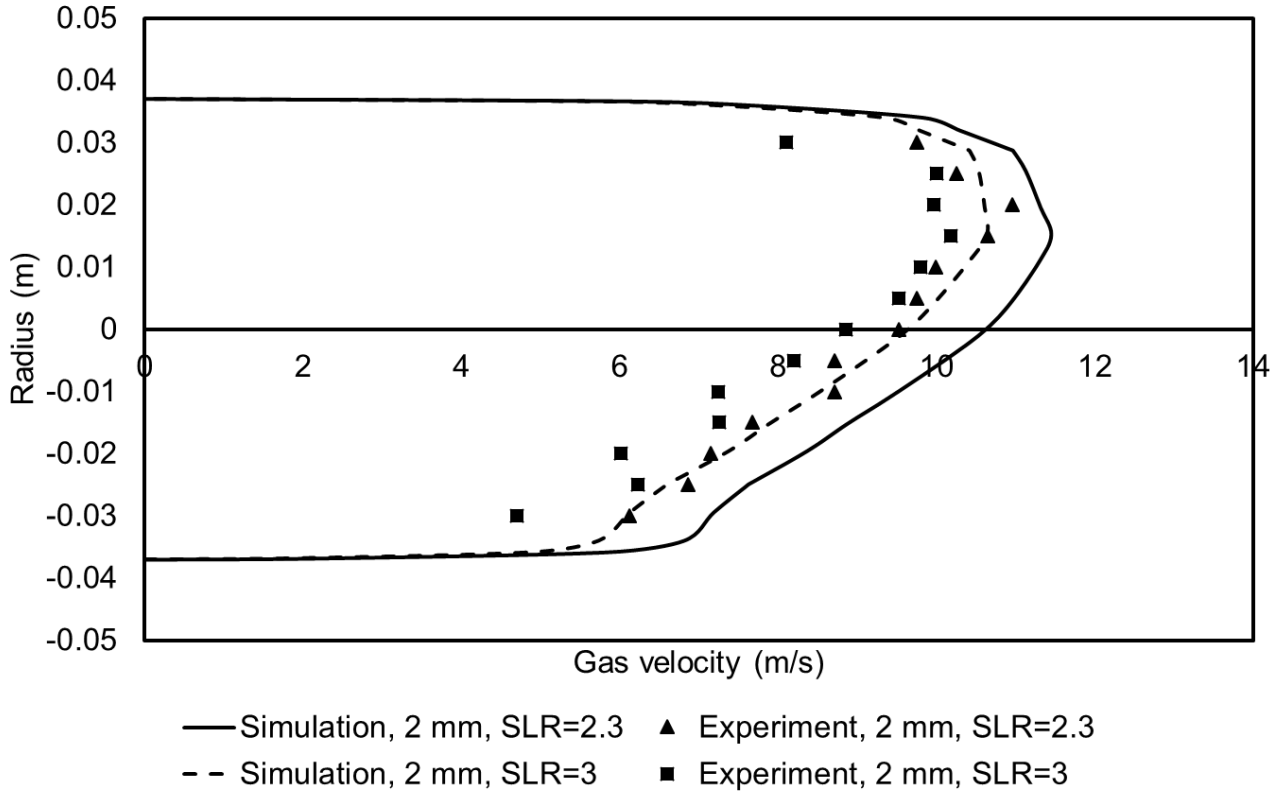

Figure. 15: Gas velocity comparison between simulation and experiment for vertical profile in the presence of 2 mm glass beads, SLR=2.3, 3, z=2 m.

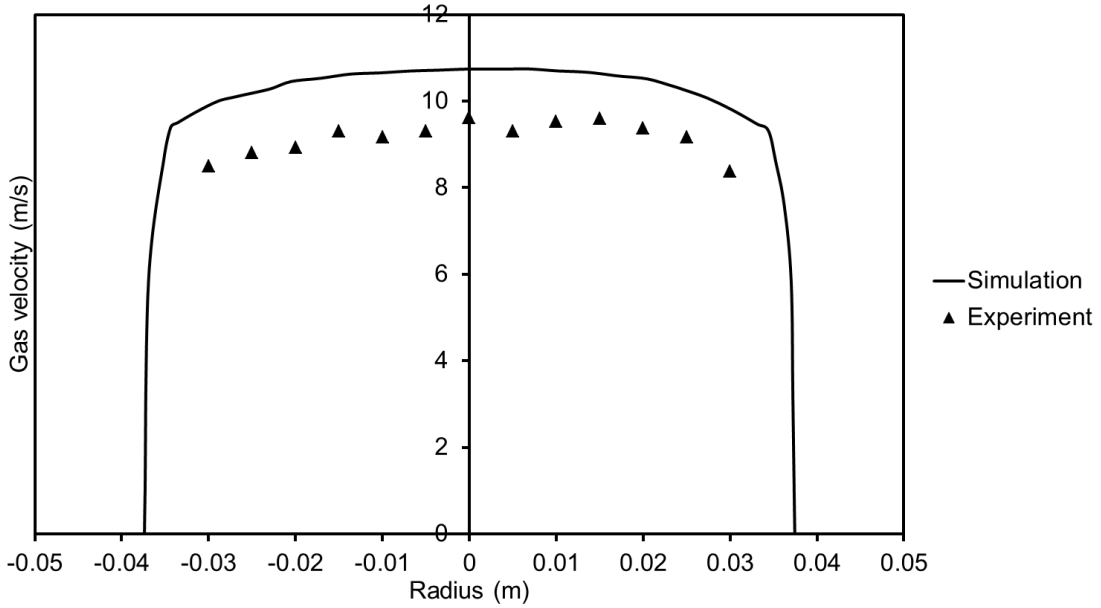

Figure. 16: Gas velocity comparison between simulation and experiment for horizontal profile in the presence of 0.8-1 mm glass beads, SLR=2.3, z=2 m.

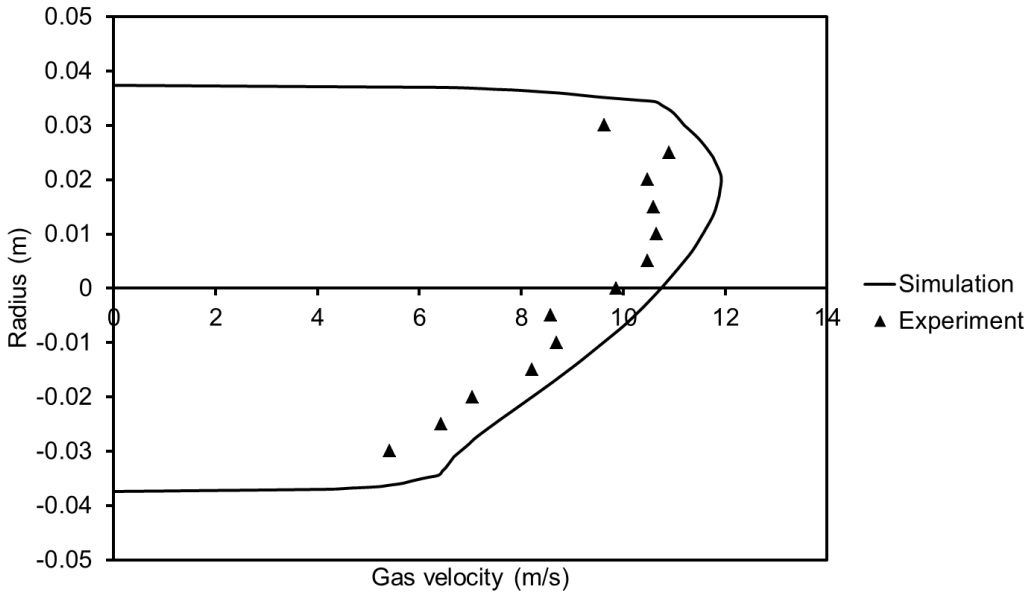

Figure. 17: Gas velocity comparison between simulation and experiment for vertical profile in the presence of 0.8-1 mm glass beads, SLR=2.3, z=2 m.

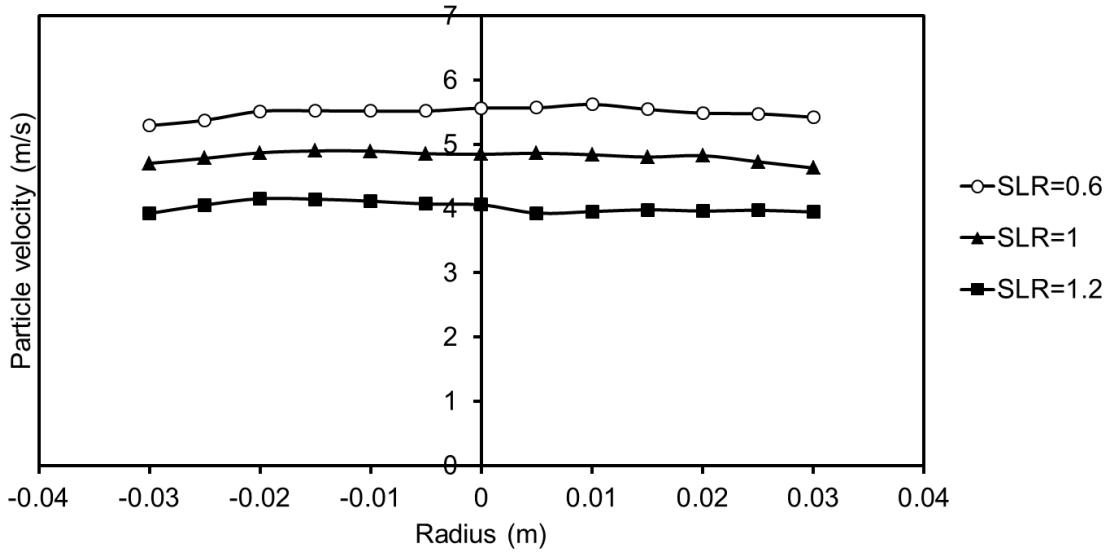

Figure. 18: Effect of solid loading ratio on the horizontal profile of mean axial isometric particle velocity, z=1 m.

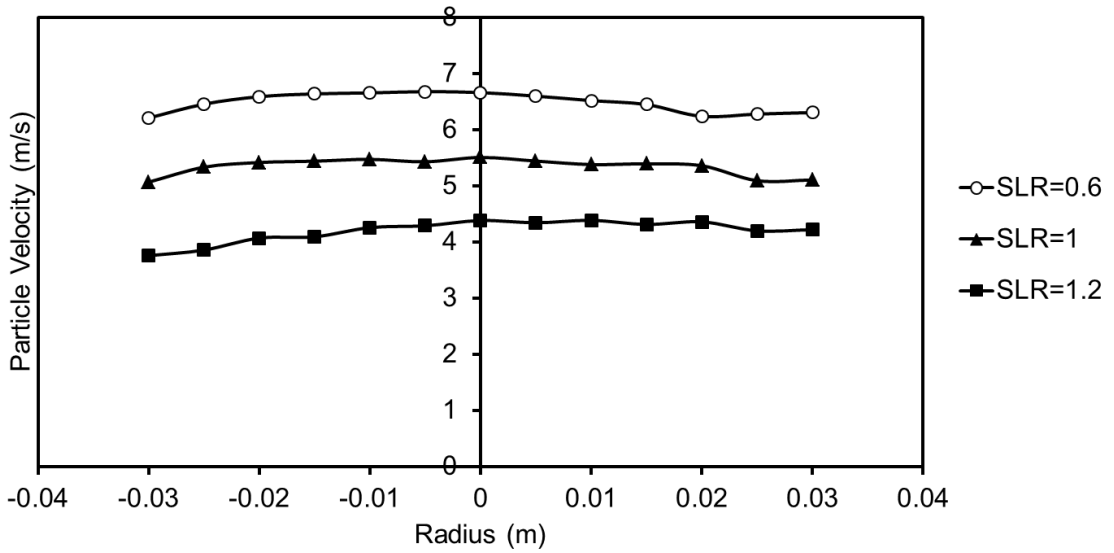

Figure. 19: Effect of solid loading ratio on the horizontal profile of mean axial isometric particle velocity, z=2 m.

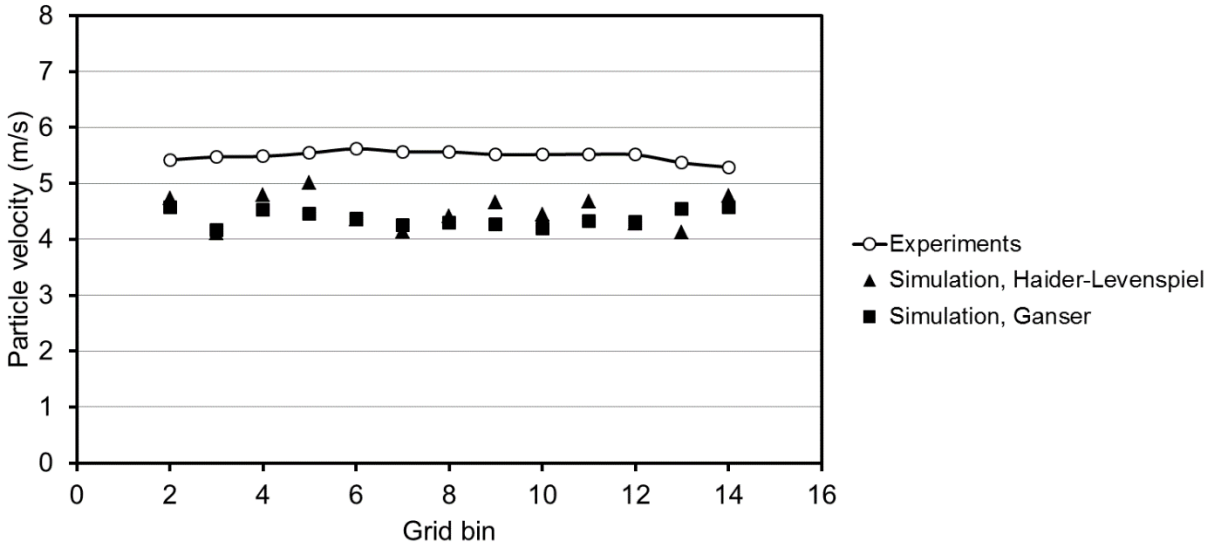

Figure. 20: Mean axial particle velocity comparison between experiment and simulation for horizontal profile of isometric particle, SLR=0.6, z=1 m.

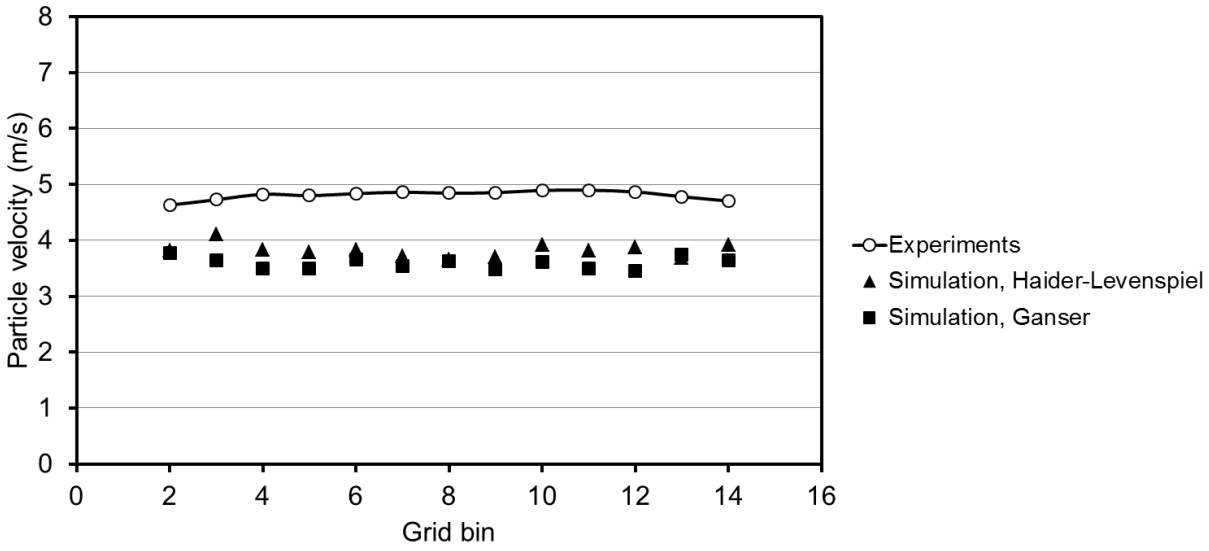

Figure. 21: Mean axial particle velocity comparison between experiment and simulation for horizontal profile of isometric particle, SLR=1, z=1 m.

Reference	Experimental rig	Test solid and flow conditions	Key results
Laín et al. [11]	Horizontal channel	• Five kinds of glass beads with mean size of 0.06, 0.1, 0.195, 0.625, 1 mm • Air velocity up to 30 m/s	1. Measured gas and particle velocities were used to validate numerical results
Laín and Sommerfeld [12]	Horizontal channel	• Glass beads, with diameter between 0.06 and 0.625 mm • Gas velocity, 20 m/s	1. Mean and fluctuating air velocity were measured in the presence of particles 2. Carrier phase turbulence intensity was attenuated due to the presence of 0.13 and 0.195 mm glass beads
Lu et al. [13]	Horizontal pipe	Glass beads, average diameter < 0.1 mm	1. An annular flow pattern was seen for axial particle velocity in a pipe cross section 2. A stratified pattern was observed for the particle number distribution over a cross section
Tsuji and Morikawa [14]	Horizontal glass pipe	• Plastic particles, 0.2 mm and 3.4 mm • Air conveying velocity 6 to 20 m/s	1. The effects of the solid particles on air flow turbulence intensity varied heavily with the particle size. The 3.4 mm particles increased the carrier phase turbulence intensity while the 0.2 mm ones reduced it 2. With adding the particle, the maximum gas velocity shifted upward from the pipe centre
Datta et al. [15]	Horizontal and vertical pipe	• Polyamide chips, approximate 3 mm long, 3 mm wide and 1 mm thick • Air velocity 1 to 5 m/s	1. The LDA technique was used to validate ECT measurements

Table 1 : The application of the LDA technique for pneumatic conveying

C_μ	$C_{\varepsilon 1}$	$C_{\varepsilon 2}$	σ_k	σ_ε
0.09	1.44	1.92	1	1.3

Table 2 : Constant values used as default in the k-ε model

Simulation method	CFD-DEM (Eulerian-Lagrangian)	
Coupling method	Two-way coupling	
FLUENT	Spherical particles	Non-spherical particles
Air density (kg/m^3)	1.225	
Air viscosity (Pa.s)	1.78×10^{-5}	
Turbulence model	k-ε model with the source terms proposed by Geiss et al. [43] and Mandø [44]	k-ε model
EDEM	Spherical particles	Non-spherical particles
Particle creation	Created in the inclined pipe with the initial velocity similar to the experiments	Created in the inclined pipe with the initial velocity similar to the experiments
Particle flow rate (kg/s)	0.1128, 0. 1277, 0.1329	0.0296, 0.04467
Poisson's ratio	0.24	0.35
Shear modulus (Pa)	2.62×10^{10}	1.2×10^{8}
Particle-Particle, Particle-wall contact model	Non-linear Hertz-Mindlin	Non-linear Hertz-Mindlin
Particle diameter (m)	0.0008-0.001, 0.0015, 0.002	0.001×0015
Particle density (kg/m^3)	2540	1140
Coefficient of restitution (particle-wall)	0.97	0.5
Coefficient of restitution (particle-particle)	0.9	0.45
Coefficient of static friction	0.154	0.5
Time step (s)	3×10^{-7}	1.5×10^{-6}
Gas-Particle interactions	Spherical particles	Non-spherical particles
Drag model	Ergun and Wen & Yu	Ganser or Haider and Levenspiel
Lift model	Magnus lift force	Magnus lift force

Table 3: Numerical parameters for pneumatic conveying simulation

Particle material	Polyamide6
Particle diameter (m)	0.001
Particle length (m)	0.0015
Particle density (kg/m^3)	1140
Aspect ratio	1.5
Particle sphericity	0.8184
Particle flow rate (kg/m^3)	0.0296, 0.04467
Gas velocity (m/s)	9.5, 8.5, 7.0
SLR	0.6, 1.0 ,1.2

Table 2: Isometric particle characteristics and experimental conditions

Particle Material and SLR	Shape	Drag Model Used	Lift Model Used	Turbulence Model Used (with/without carrier phase modulation)	Rellative discrepency between simulation and experiment (%) (Horizontal Profile	Relative discrepancy between simulation and experiment (%) Vertical profile
2 mm glass beads, SLR= 2.3	Spherical	Ergun-Wen & Yu	Magnus	k-ε with modulation	22	25
2 mm glass beads, SLR= 3	Spherical	Ergun-Wen & Yu	Magnus	k-ε with modulation	35	35
1.5 mm glass beads, SLR= 2.3	Spherical	Ergun-Wen & Yu	Magnus	k-ε with modulation	25	25
1.5 mm glass beads, SLR= 3	Spherical	Ergun-Wen & Yu	Magnus	k-ε with modulation	33	38
1.5 mm glass beads, SLR= 3.5	Spherical	Ergun-Wen & Yu	Magnus	k-ε with modulation	55	36
0.8-1 mm glass beads, SLR= 2.3	Spherical	Ergun-Wen & Yu	Magnus	k-ε with modulation	40	36
Cylindrical particles, SLR=0.6	Non-spherical	Di Felice (Ganser)	Magnus	k-ε unmodulated	20	-
Cylindrical particles, SLR=1	Non-spherical	Di Felice (Ganser)	Magnus	k-ε unmodulated	25	-
Cylindrical particles, SLR=0.6	Non-spherical	Di Felice (Haider-Levenspiel)	Magnus	k-ε unmodulated	18	-
Cylindrical particles, SLR=1	Non-spherical	Di Felice (Haider-Levenspiel)	Magnus	k-ε unmodulated	20	-

Table 5: Summary of discrepancy between experiment and simulation for all cases